Controlled Fabrication of Opal Structured Janus Hydrogel Microparticles via Sequential Micromolding

A thesis submitted by

Lauren Tice

In partial fulfillment of the requirements

for the degree of

Master of Science in

Bioengineering

TUFTS UNIVERSITY

May 2017

Advisor: Hyunmin Yi

Abstract

Hydrogel microparticles containing synthetic opal structures via closely packed nanoparticles hold significant potential for reagentless detection in biosensing, medical diagnostics, and environmental monitoring. Yet there exist technical hurdles in reliable, simple, and readily tunable fabrication of such microparticles. This thesis examines critical parameters in the robust fabrication and characterization of opal structured hydrogel microparticles via a two-step micromolding technique. Parameters examined include evaporation rate, surfactant addition, polystyrene bead size, and various polymer systems toward uniform and intense color. I demonstrated these microparticles display uniform and intense color when fabricated with poly(ethylene glycol) diacrylate. Scanning electron micrographs and Bragg Equation analysis show the opal layer packing influences microparticle color, indicating uniform color arises from minimizing simple cubic packing. The studies represent significant progress towards consistent and robust fabrication of these microparticles which have considerable potential in biosensing applications without using optical reagents or separate tags for inexpensive detection of multiple variables.

Table of Contents

List of Figures

List of Equations

1. Introduction

Synthetic opals are ordered structures of silica[11], latex, or polymer[12] spheres in nanometer sizes. If the refractive index is large, a photonic band gap is formed where different wavelengths of light are unable to proceed through the material[15]. This inhibition of various wavelengths creates visible color changes in the synthetic opal. Opal structured materials hold significant potential for reagentless detection in numerous applications such as biosensing, medical diagnostics, and environmental changes due to their color changing capabilities based on environmental deviations. There have already been advances in the use of synthetic opal materials in optical limiters, lasers, filters[1], chemical sensors, data storage[2], and membranes[3].

There also has been an increase in the development of reliable fabrication methods for synthetic opal structured materials as they have gained much attention in the scientific community due to their photonic nature. Two common fabrication methods for synthetic opals are self-assembly, which can utilize electrostatic, gravitational, or capillary forces, and lithography such as soft lithography or nanoimprint lithography[2]. However, these technologies have some critical limitations such as limited starting materials with the appropriate size and composition, complexity of the procedure when a template is involved, and a limited quantity of synthetic opals produced[7].

Meanwhile, polymeric hydrogel microparticles also hold significant potential in medical diagnostics and biosensing applications. Hydrogels are crosslinked polymers consisting of hydrophilic chains. Some of their advantages include rapid solution-like kinetics, tunable properties, non-fouling nature, and rapid assay time[4]. There have been recent advances in the fabrication of polymeric hydrogel microparticles such as shape-encoded and multicompartmental

microparticles which have allowed rapid multiplexed sensing and diagnostic assays. Fabrication techniques include flow lithography, contact photolithography, and capillary microfluidic devices[5]. Despite such advances in these areas, there still exist challenges in the fabrication process of polymeric hydrogel microparticles. For example, microfluidic techniques lack scalability and control over the flow, involve harsh and extensive cleaning processes, and require expensive equipment[6].

Combined, opal structured hydrogel microparticles have a wide range of potential applications in medical diagnostics and biosensing. As a result, there exists a need for reliable fabrication methods of opal structured hydrogel microparticles that are reproducible and result in a high yield of uniform microparticles with intense color.

In this thesis, I demonstrate the use of micromolding in a sequential manner to fabricate opal structured hydrogel microparticles to address the challenges mentioned above. Micromolding is advantageous because it is easily controlled, reliable, and inexpensive[22]. A schematic of the simple two-step micromolding-based fabrication process of opal structured hydrogel microparticles I exploited in this thesis is shown in Figure 1.

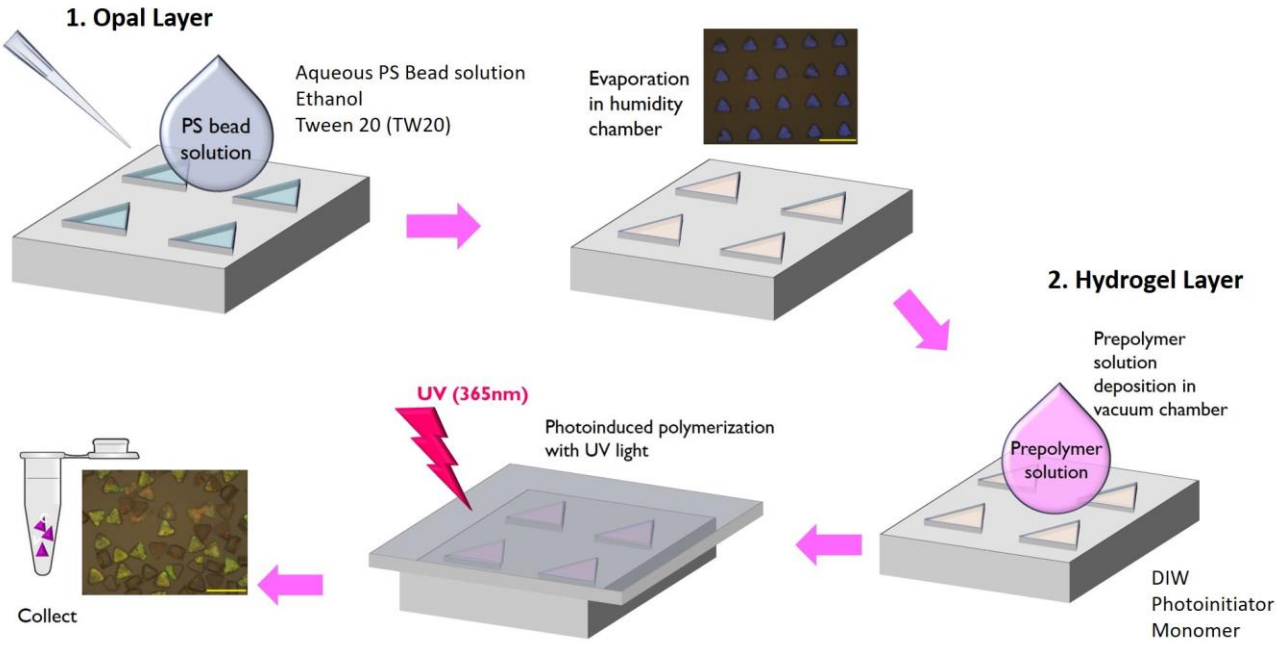

Figure 1. Two-step fabrication process for opal structured hydrogel microparticles.

Briefly, the first step is to fill various shaped wells of a polydimethylsiloxane (PDMS) micromold with a polystyrene (PS) bead solution containing aqueous PS beads, tween 20 (TW20), and ethanol in a humidity-controlled chamber. Next, a prepolymer solution containing photoinitiator, a polymer system of either polyacrylamide or poly(ethylene glycol) diacrylate (PEGDA), and deionized (DI) water is placed onto the micromold and left in a vacuum chamber, allowing the prepolymer solution to seeps into the wells. The excess prepolymer solution is removed before placing a cover slide on top of the micromold and then under a handheld UV light (365nm) to induce polymerization, forming crosslinked opal structured hydrogel microparticles. The cured microparticles are then removed from the micromold and collected.

Various important parameters were examined such as the evaporation rate, use of surfactants, polystyrene bead size, and various polymer systems for reliable deposition of PS beads, resulting in intense and uniform opal structured hydrogel microparticles with a high yield

using the two-step sequential micromolding process outlined above. The results show TW20 is required in the PS bead solution which needs to be deposited into the wells in a humidity-controlled chamber. Additionally, the color of the opal layer is dependent on the size of the PS beads and using PEGDA as the polymer system results in a high yield of intense and uniformly colored microparticles. Both a modified version of the Bragg Equation and scanning electron microscopy (SEM) were used to characterize the packing structure of the PS beads which needs to be controlled to achieve uniform color. These findings represent an important step forward in the fabrication of opal structured hydrogel microparticles in a simple and reproducible manner. They have the potential to be used in biosensing applications without the use of optical reagents or separate tags for low cost detection of multiple variables.

2. Background

2.1 Opals

Opals are naturally occurring gemstones that are most abundant in volcanic rocks[8]. They can also be found near hot springs where they are deposited by hydrothermal solutions at low temperatures[9]. Opals are comprised of $SiO_2 \cdot nH_2O$ which is silicone oxide and n amount of water between the ordered structure of silicone spheres[8]. They are colorless, however when the stone is viewed from different angles various colors such as yellow, blue, green, and red are clearly visible by the naked eye as shown in Figure 2.

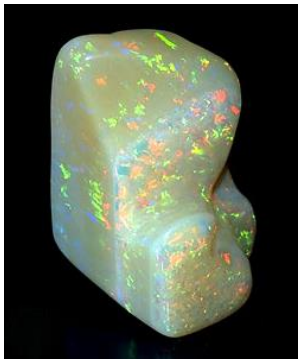

Figure 2. Opal gemstone with various colors visable[8].

This play of colors is caused by white light diffraction. When white light hits the opal, it strikes the silica spheres and voids of the opal's structure. The light is then diffracted at different wavelengths, resulting in the observation of multiple colors on the surface of the opal[9].

2.2 Synthetic Opals

Opals can be synthetically fabricated and have gained much attention in the scientific community due to their photonic nature. Similar to natural opals, synthetic opals or photonic crystals diffract photons. If the refractive index is large, a photonic band gap is formed where different wavelengths of light are unable to proceed through the crystal[15]. This inhibition of various wavelengths creates color changes in the synthetic opal. Synthetic opals therefore provide

numerous useful applications such as optical integrated circuits, light emitting diodes, and sensors[15].

Common materials for synthetic opals are monodisperse particles made from latex, silica[11], or polymer such as polystyrene[12]. The result is synthetic opal with a face centered cubic structure (FCC)[12]. There are two common methods to fabricate synthetic opals: self-assembly and lithography[10].

2.2.1 Self-Assembly

Self-assembly is typically less expensive and a less tedious process than lithography. However self-assembly relies on chemical techniques which may make this fabrication method challenging as irregularities in the packing structure may occur, resulting in other packing structures instead of FCC[12]. The general procedure to make synthetic opals by self-assembly is illustrated in Figure 3 below.

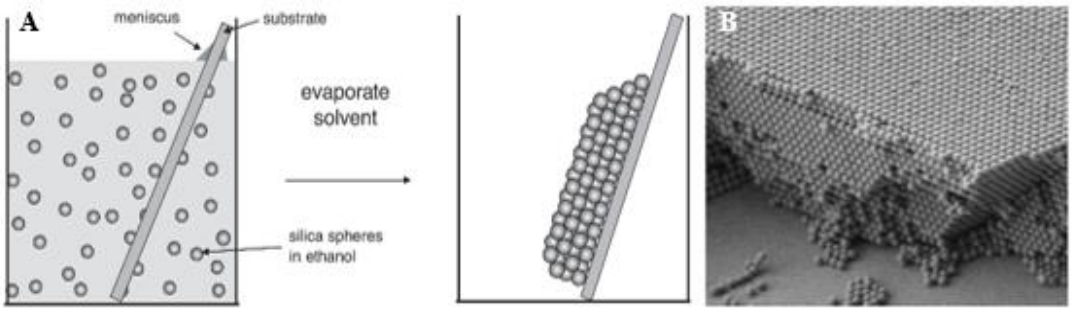

Figure 3. (A) Schematic diagram for the fabrication of synthetic opal by self-assembly and (B) resulting synthetic opal made from silica spheres[13].

Monodisperse spheres in micro or nanometer sizes are made from silica, latex, or polymer and are dispersed within a solvent containing a substrate in the solution. As the solvent is left to evaporate and under favorable correct conditions, the monodisperse spheres will adhere to each

other and deposit onto the substrate in a FCC structure with uniform thickness, thus creating synthetic opal[13].

2.2.2 Lithography

Synthetic opals can also be fabricated using lithographic methods, such as soft lithography. Lithography, or the "top-down" approach, involves the etching of small patterns onto a material with extreme precision[14] through replica molding, microcontact printing or other methods[15]. Replica molding, more specifically micromolding, is the method used in this study to produce synthetic opals.

2.3 Inverse Opals

Inverse opal structures can be made which also display synthetic opal properties such as color changes[15]. Inverse opal is simply the structure void space between the spheres as shown in Figure 4B.

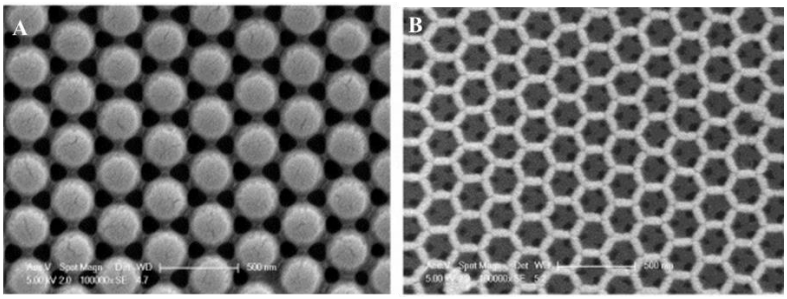

Figure 4. (A) SEM images of synthetic opals made from polymer spheres and (B) silica synthetic inverse opal made from polymer spheres[10].

Synthetic opal and inverse opal share a similar FCC packing structure, with opal displaying spheres and inverse opal displaying voids, as shown in the SEM micrographs of Figure 4A and 4B. To fabricate inverse opal, the void spaces of synthetic opal are filled in with a dielectric material and the spheres are then removed by wet chemical etching or calcination depending on the material of

the spheres[9]. This leaves behind the void spaces between the spheres. Depending on the intended application, inverse opals may be more preferred over synthetic opals due to their more complete photonic band gap[10].

2.4 Polymeric Hydrogels

2.4.1 Applications

Polymeric hydrogels are three-dimensional networks comprised of hydrophilic crosslinked polymers. They can trap large volumes of water by capillary forces and surface tension[17] due to their porous structure and hydrophilicity[18]. They are biocompatible, and have highly tunable properties[12]. For example, in some hydrogels the degree of swelling can be tuned by changing the pH, ionic strength, light, temperature, pressure, and electric and magnetic fields in their environment[20]. As a result, hydrogels are used in a wide range of applications such as media for storage, tissue engineering, matrix chemistry, drug delivery[17], contact lenses, artificial organs, and sensors[20].

2.4.2 Fabrication

Polymeric hydrogels can be fabricated by numerous covalent reactions including Schiff base formation, Michael type addition, enzyme-catalyzed reactions, photopolymerization of thiol and terminal alkenes, and free radical chain photopolymerization[17]. In this thesis, free radical chain photopolymerization was the fabrication method used.

Free radical chain photopolymerization is comprised of three stages: initiation, propagation, and termination as shown in Figure 5.

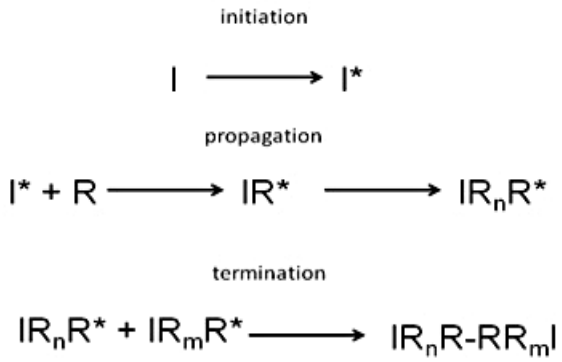

Figure 5. Free radical chain photopolymerization mechanism of initiation, propagation, and termination, where I is an initiator and R are the monomer units. A star (*) represents a free radical[21].

During the initiation step, initiator molecules split to form two free radicals which are highly reactive species with unpaired electrons. The propagation step occurs next where a free radical combines with a monomer unit, forming the beginning of the growing polymer chain and an active center which can attack other monomers. The free radical is then propagated down the growing polymer chain as more monomer units are added. The final step, termination, is when the polymer chain stops growing, thus creating the final product. Termination can occur when the two chains combine, a reaction occurs with an impurity, or in the absence of monomers[16]. Advantages of using free radical chain photopolymerization include rapid polymerization rate, low polymerization temperatures, and lack of solvents[14].

2.4.3 Micromolding Technique

Micromolding, also called imprint lithography, is the method utilized in this thesis for fabrication of opal structured hydrogel microparticles. Micromolding is generally comprised of three steps. First a liquid UV-curable monomer is poured over a polymeric substrate which is a master mold containing a pattern for the microparticles. Next, the mold is exposed to UV light to

induce crosslinking and form the microparticles in the wells of the mold. Finally, the microparticles are removed from the mold[19].

While there are other methods for microparticle fabrication such as contact lithography and flow lithography[19], micromolding offers many advantages. It produces duplication of three-dimensional topologies in a single step and enables complex structures in the master to be duplicated into many copies in a way that is simple, easily controlled, reliable, and inexpensive[22]. Due to these advantages, micromolding has been used for the mass production of many objects such as holograms, compact disks (CDs), microtools, and diffraction gratings[22]. Micromolding using a polydimethylsiloxane (PDMS) micromold was the technique used in this thesis to fabricate opal structured hydrogel microparticles.

3. Materials and Methods

3.1 Materials

Polystyrene beads were fabricated by our collaborator Mr. Jun Hyuk Lee at Professor Piljin Yoo's group of Sungkyunkwan University in Korea. Poly(ethylene glycol) diacrylate (PEGDA, average Mn 700 Da), acrylic acid (AA) anhydrous (180−200 ppm MEHQ inhibitor, 99%), and 2-hydroxy-2-methylpropiophenone (Darocur 1173, photoinitiator, PI) were purchased from Sigma-Aldrich (St. Louis, MO). Acrylamide (AAm) (99.9%), tween 20 (TW20), sodium dodecyl sulfate (SDS), and poly(dimethylsiloxane) (PDMS) elastomer kits (Sylgard 184) were purchased from Thermo Fisher Scientific (Waltham, MA). N,N′-Methylenebis(acrylamide) (bisacrylamide) was purchased from EMD Millipore (Billerica, MA). Ethanol (190 proof) was purchased from Decon Laboratories (King of Prussia, PA). All chemicals were analytical grade and used without further purification.

3.2 Fabrication of Opal Structured Hydrogel Microparticles

The first step to fabricate opal structured hydrogel microparticles was to make a PDMS micromold containing 40x40 circle, square, triangle, hexagon, or pentagon shaped micromolds. This was done by thermal curing of Sylgard 184 elastomer with 10% (w/w) crosslinking agent upon overnight incubation at 65ºC on a silicon master mold. Next the PS bead solution was prepared by mixing aqueous PS beads of varying sizes, 190 proof ethanol (20-50% v/v), and TW20 (0.1 - 0.3% v/v) by pipetting up and down. The PDMS mold was then covered with the PS bead solution in a humidity-controlled chamber (~92% relative humidity) to slowly evaporate the ethanol and water in the solution. The air bubbles were removed from the microwells by scratching the mold with a disposable pipette tip so that the PS bead solution seeped into the microwells. The

excess PS bead solution was removed with a pipette and the mold was left in the humidity-controlled chamber so the PS beads could assemble as the ethanol and water slowly evaporated.

Next the prepolymer solution was prepared by mixing either acrylamide and bisacrylamide (20 - 40% total monomer content, T, with either 29:1, 19:1, or 4:1 ratio of acrylamide to bisacrylamide) or 20% (v/v) PEGDA with 1% (v/v) Darocur 1173 photoinitiator, 1% (v/v) acrylic acid, 0.1% (v/v) TW20, and deionized (DI) water using vortex mixer (1 minute) and sonicator (5 minutes). The PDMS mold was then covered with the prepolymer solution and left in a vacuum chamber for 25 minutes to remove air bubbles in the microwells, allowing the prepolymer solution to seep in. The PDMS mold was then placed in a humidity-controlled chamber where excess prepolymer solution was removed with a pipette and a cover slide was placed over the top of the mold to prevent evaporation of the prepolymer solution in the microwells. Afterwards, the PDMS mold was placed under a 365 nm UV light with an 8W hand-held UV lamp (Spectronics Corp., Westbury, NY) to cure the hydrogel layer for 45 minutes for acrylamide or 15 minutes for PEGDA. The polymerized microparticles were then collected by pipetting and physically bending the mold and then washed 3 times with DI water containing 0.05% (v/v) TW20.

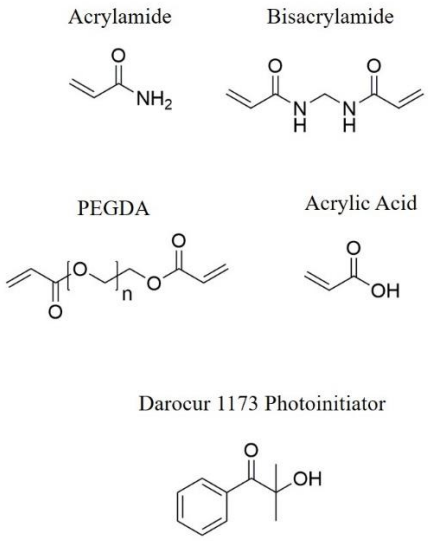

Figure 6. Chemical structures of acrylamide, bisacrylamide, PEGDA, acrylic acid, and Darocur 1173 photoinitiator. In this thesis, PEGDA with a molecular weight of 700 was used.

3.3 Imaging Analysis

The microparticles were imaged in DI water with an epifluorescence microscope (Olympus BX51 equipped with a DP70 microscope digital camera, Center Valley, PA) with a 10x objective and coming light from the top of the microscope.

3.4 Scanning Electron Microscopy (SEM) Analysis

To prepare the PS beads for SEM imaging, the PS bead solution was prepared and deposited on to a PDMS mold as described above. The mold was then placed on a stub and sputter coated (The 108 Auto Sputter Coater, Ted Pella, Inc., Redding, CA) with a thin layer of gold–palladium for 30 seconds. To prepare the opal structured hydrogel microparticles for SEM imaging, 10µL of the microparticles in DI water was placed onto a stub and left in ambient conditions until the water evaporated. They were then sputter coated (The 108 Auto Sputter Coater, Ted Pella, Inc., Redding, CA) with a gold–palladium layer for 10 seconds. The morphology of the PS beads and microparticles was characterized using a JEOL 5910 scanning electron microscope (SEM) operating at 5 kV.

4. Results and Discussion

4.1 Effect of evaporation rate and ethanol content on the uniform deposition and color of the opal layer

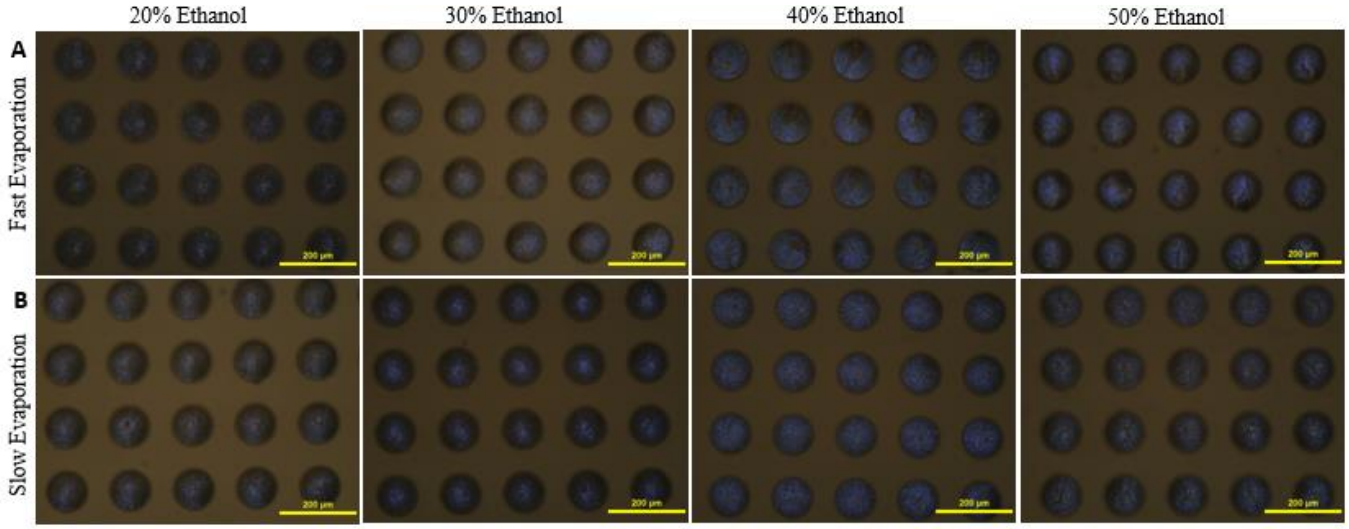

Figure 7. Deposition of the opal layer with varying evaporation rates and ethanol content. (A) brightfield micrographs of the opal layer with fast evaporation in dry conditions of the PS bead solution with varying ethanol contents of 20% - 50%. (B) Brightfield micrographs of the opal layer with slow evaporation in wet conditions of the PS bead solution with varying ethanol contents of 20% - 50%.

First, I examined the effect of evaporation rate and ethanol content for controlled assembly of PS beads toward uniform color as the first fabrication step of the opal layer deposition, as shown in Figure 7. The hypothesis for the varying evaporation rate is that slowly evaporating the PS bead solution in a humidity-controlled chamber (~90% relative humidity) provides the PS beads with more time to arrange into closely packed face-centered cubic (FCC) structure, the most stable packing structure with the highest packing factor. Thus, this structure would potentially result in the most uniform color. To promote FCC packing, I hypothesized that adding varying amounts of ethanol would control and minimize non-uniform evaporation due to the meniscus of water, thus allowing for more uniform packing of the PS beads.

For this, I added aqueous PS bead solution with varying concentrations of ethanol from 20 to 50% (v/v) onto PDMS micromolds with wells that define the shapes of the microparticles. Upon removing excess PS bead solution, I then exposed the micromolds to either dry or wet conditions for varying drying times. The resulting PS bead layers were imaged via brightfield microscopy with white light.

First, the optical micrographs in Figure 7A show that fast evaporation leads to non-uniform color regardless of the ethanol content in the PS bead solution. This suggests that the PS beads did not have sufficient time to assemble into uniform arrangements (i.e. FCC). In contrast, Figure 7B shows that slow evaporation of the PS bead solution with 40% ethanol in a humidity-controlled chamber leads to intense and uniform blue color within each microwell and among multiple microwells. Meanwhile, PS bead solutions with 20, 30, and 50% ethanol yield non-uniform color, suggesting the existence of optimal solution compositions for uniform color formation. Compared with Figure 7A, this result clearly indicates drying time may be a crucial factor in the uniform assembly of PS beads. Meanwhile, evaporation of pure aqueous PS bead solution leads to lack of uniform color, similar to the results in Figure 7A (data not shown), confirming the need for ethanol in promoting uniform packing.

In short summary, the results in Figure 7 show that slow evaporation of PS bead solution containing 40% ethanol produces uniform and intense blue color without any pigment or dye, presumably due to the well-controlled close packing of the PS beads and the resulting light diffraction. The results also support the hypothesis that when the PS bead solution is evaporated slowly in the presence of ethanol, the resulting color is brighter and more uniform.

4.2 Effect of surfactant in the PS bead solution on the uniform deposition and color of the opal layer

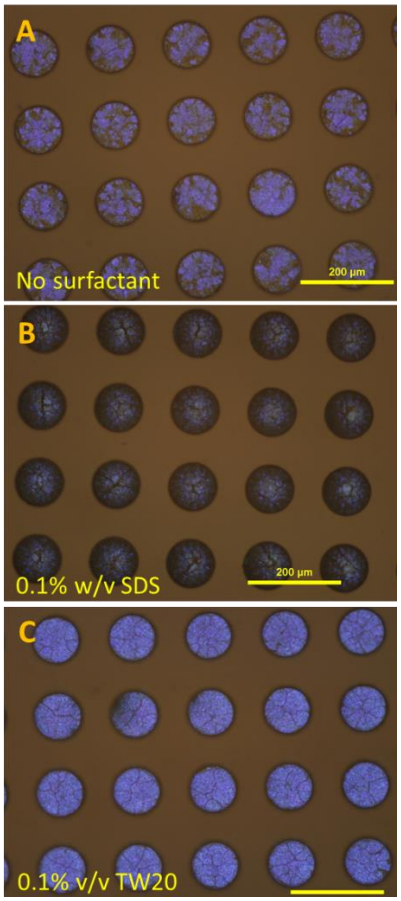

Figure 8. Deposition of the opal layer imaged with brightfield microscopy with (A) no surfactant, (B) 0.1% (w/v) sodium dodecyl sulfate (SDS), and (C) 0.1% (v/v) tween 20 (TW20) with 40% ethanol in the PS bead solution.

I next examined the effect of using various surfactants in the PS bead solution for deposition of the PS beads towards uniform and intense color. The hypothesis here is that surfactants would minimize surface tension among PS beads and of the PS bead solution, leading to more uniform packing and color.

To do this, I separately added 0.1% (v/v) tween 20 (TW20) and 0.1% (w/v) sodium dodecyl sulfate (SDS) into the PS bead solution containing 40% (v/v) ethanol and allowed the PS beads to

slowly evaporate in the humidity-controlled chamber. The resulting PS bead layers were imaged via brightfield microscopy with white light.

Figure 8A shows that the deposition of PS beads without any surfactant results in some areas of bright but non-uniform blue color within each individual well. In contrast, Figure 8B shows deposition using SDS in the PS bead solution results in dark and non-uniform blue color. Deposition with TW20 in the PS bead solution, as shown in Figure 8C, results in a uniform and intense blue color.

The results indicate using TW20 in the PS bead solution results in a uniform and intense blue color. They also suggest the use of different surfactants in the PS bead solution leads to different packing structures, and thus color. TW20 is a branched polyethylene glycol (PEG)-based, non-ionic surfactant. While the exact mechanism of its effect is not clear, TW20 should help lower surface tension further so that the PS beads can settle and assemble into FCC structure better, resulting in a more intense and uniform color.

In short summary, the results in Figure 8 indicate that polymeric surfactant TW20 has a favorable effect on the color of the deposited PS layer, presumably due to substantially improved uniformity of the packing by reduced surface tension.

4.3 Effect of varying TW20 concentrations in the PS bead solution on uniform color and deposition of the opal layer

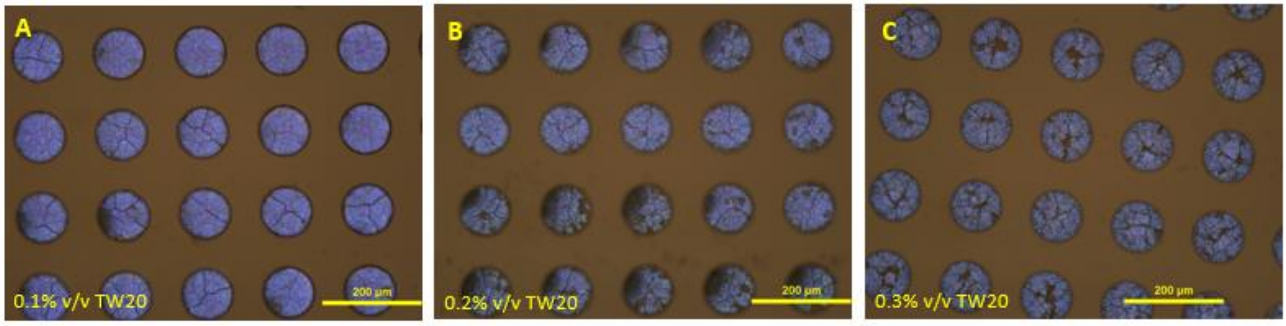

Figure 9. Deposition of the opal layer imaged with brightfield microscopy with (A) 0.1% v/v TW20, (B) 0.2% v/v TW20, and (C) 0.3% v/v TW20 in the PS bead solution containing 40% ethanol.

I next examined the effect of varying concentrations of TW20 in the PS bead solution on uniform deposition and color of the PS beads. The hypothesis was that higher concentrations of TW20 would lead to more uniform and intense color.

For this, I separately added varying concentrations of 0.1% - 0.3% (v/v) TW20 to the PS bead solution consisting of 40% (v/v) ethanol and allowed the PS bead solution to slowly evaporate in a humidity-controlled chamber under identical deposition conditions, and imaged the resulting PS bead layers under identical imaging conditions as in the results above.

The results in Figure 9A show that when 0.1% (v/v) TW20 is used, the result is intense and uniform blue color, consistent with the results shown in Figure 8 above. Conversely when 0.3% (v/v) TW20 is used, as shown in Figure 9C, the color is a non-uniform blue color with many brown areas. The color and uniformity of using 0.2% (v/v) TW20 shown in Figure 9B is some brown

areas interspersed in a somewhat uniform blue color. Therefore, higher concentrations of TW20 in the PS bead solution results in non-uniform deposition of the PS beads.

The results show using 0.1% (v/v) TW20 in the PS bead solution results in an intense and uniform blue color. Increasing concentrations of TW20 lead to more brown areas and less intense color. The exact mechanism of TW20 is unclear but higher content of TW20 seems to disrupt the uniform deposition of the PS beads and perhaps prevents the beads from settling into a FCC structure, thus resulting in areas of brown and less intense blue color.

In summary, the results in Figure 9 indicate a favorable concentration of TW20 in the PS bead solution is 0.1% (v/v) TW20 to reduce the surface tension and improve the uniformity, resulting in an intense and uniform blue color.

4.4 Characterization of the deposition of various PS bead sizes

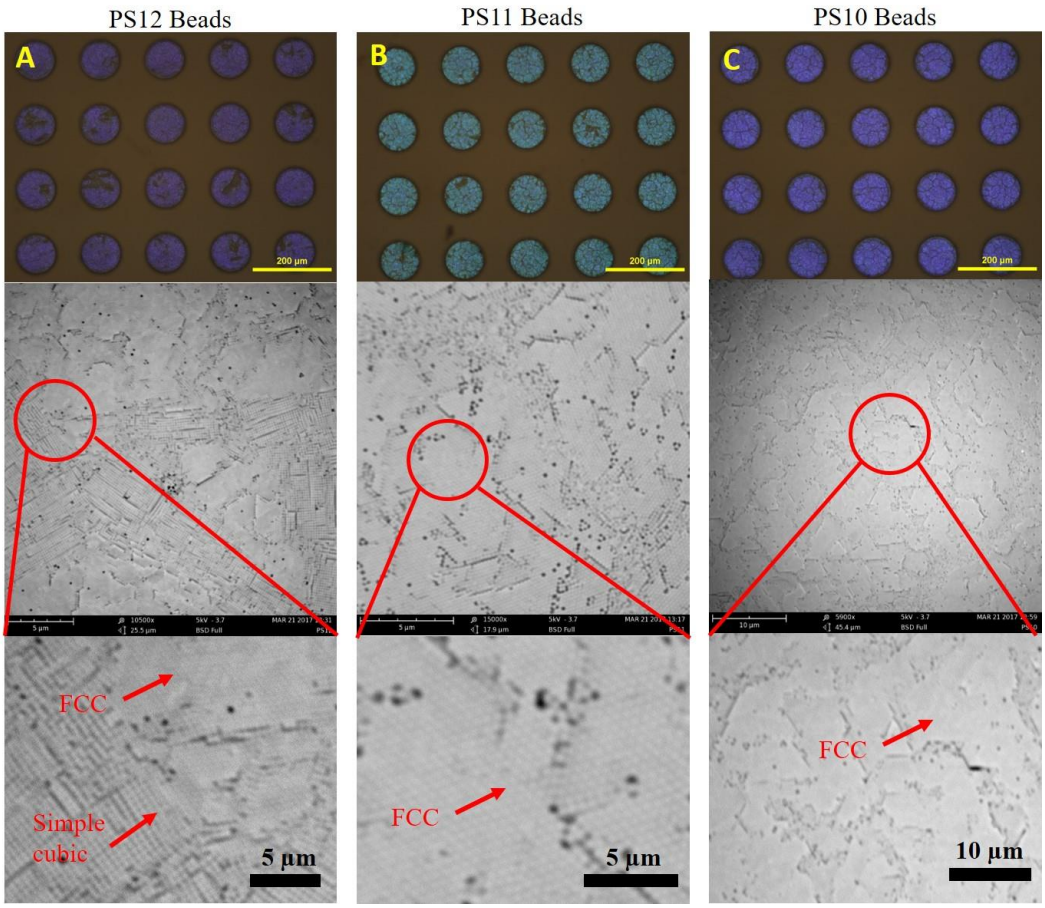

Figure 10. Deposition of the PS bead solution containing (A) PS12 beads, (B) PS11 beads, and (C) PS10 beads and their corresponding SEM images below.

I next studied the deposition of various PS beads sizes, fabricated in different batches: PS12, PS11, and PS10. The aqueous PS bead solutions were supplied in different synthesis batches by our collaborator Mr. Jun Hyuk Lee at Professor Piljin Yoo's group of Sungkyunkwan University in Korea. As different batches of the PS bead solutions have different sizes, I next studied the effect of the PS bead size on the color and assembly behavior.

To do this I deposited three PS bead solutions (PS 12, 11, 10) containing 40% (v/v) ethanol, 0.1% (v/v) TW20, and separately added the three different PS beads onto micromolds. After the

beads slowly evaporated in a humidity-controlled chamber, the molds were imaged via brightfield microscopy as shown in the top row of Figure 10. I then sputter coated the molds with a gold-palladium layer for 30 seconds and imaged them via scanning election microscopy (SEM) as shown in the bottom two rows of Figure 10.

Figure 10A shows the deposition of the PS bead solution containing PS12 beads results in mostly deep purple color with a few areas of brown. Conversely, Figure 10B shows that the PS11 bead solution produces a teal blue opal layer. Using PS10 beads results in an intense blue opal layer as shown in Figure 10C. While the aqueous PS bead solutions were fabricated with a target diameter of 200nm, the differing colors are likely due to different PS bead sizes. The diameter of the PS beads can be roughly estimated.

The diameter of the PS beads is directly proportional to the wavelength of the diffracted light and therefore color of the PS beads. This can be seen in the following modified Bragg Equation for FCC packing structures, found in the literature by Michael DeCortin[26]:

$$\lambda = \frac{\sqrt{8}}{\sqrt{3}} * D * \sqrt{n_{ps}^2 \phi + n_{void}^2 (1 - \phi)}$$

Equation 1. Modified Bragg Equation for FCC packing[26].

Where D is the diameter of the PS beads, n_{ps} is the refractive index of PS which is 1.5916, n_{void} is the refractive index of the void space which is air in this case and is 1.0003, and ϕ is the packing factor which is 0.74 for face centered cubic packing. Substituting those values into the equation results in:

$$\lambda = 2.386 * D$$

Equation 2. Simplified Modified Bragg Equation for FCC packing.

This means the wavelength is directly proportional to the diameter of the PS beads. Rough estimates of the bead diameters can be calculated using the wavelength that corresponds to each color in the visible spectrum as shown in Figure 11 below.

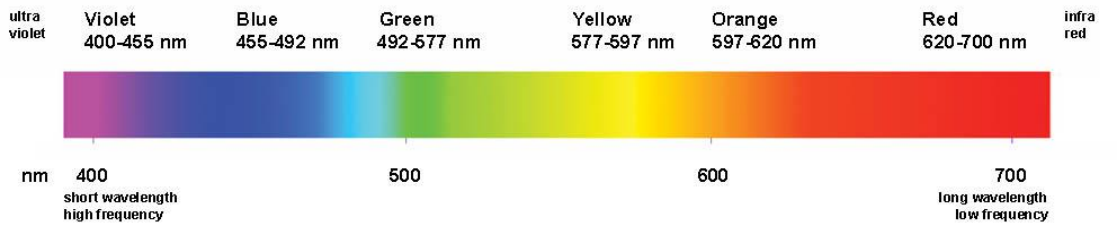

Figure 11. Colors in the visible spectrum with their corresponding wavelengths of light[23].

Purple or violet, resulting from the use of PS12 beads, has a wavelength of 400nm. Substituting the wavelength into Equation 2 above results in a diameter of about 168nm. Teal, from PS11 beads, has a wavelength of about 500nm. Using Equation 2 gives an estimate of 210nm for the diameter of the PS11 beads. Finally, blue, from PS10 beads, has a wavelength of 475nm which results in about 200nm diameter. Therefore, using the modified Bragg Equation results in the diameter of PS11 beads being the largest, followed by PS10 beads, and PS12 beads as the smallest.

The second and third rows of Figure 10 are SEM images of each of the PS beads. The SEM images depict two different packing structures: face center cubic (FCC) and simple cubic as shown by the red arrows. Both packing structures can be seen in the third row of Figure 10A where

the PS12 beads deposited in both FCC and simple cubic packing structures. The corresponding SEM images for the PS11 beads in Figure 10B show FCC structure. Finally, Figure 10C exhibits the SEM images of the PS10 beads which clearly show regions of FCC packing structure.

Hexagonal close packing leads to FCC structure. They have the same packing factor, however FCC structure has an additional third plane compared to hexagonal close packing as hexagonal close packing is one of the derivatives of FCC structure[25]. The regions of simple cubic structure seen in the last row in Figure 10A are presumably due to insufficient time or energy for the PS beads to find slots to closely pack into. The PS bead solution is very slowly evaporated in the humidity-controlled chamber, providing time for the PS beads to pack close together. However not all the PS beads have ample time to settle into FCC structure before the PS bead solution evaporates, thus producing areas of simple cubic structure or hexagonal close packing instead.

In summary, the results in Figure 10 and the modified Bragg Equation indicate the color of the PS bead deposition is directly dependent on the size of the PS beads, with smaller PS beads leading to more purple color and larger PS beads being closer to the green end of the visible light wavelength spectrum.

4.5 Effect of acrylamide as the monomer for the hydrogel layer of opal structured hydrogel microparticles

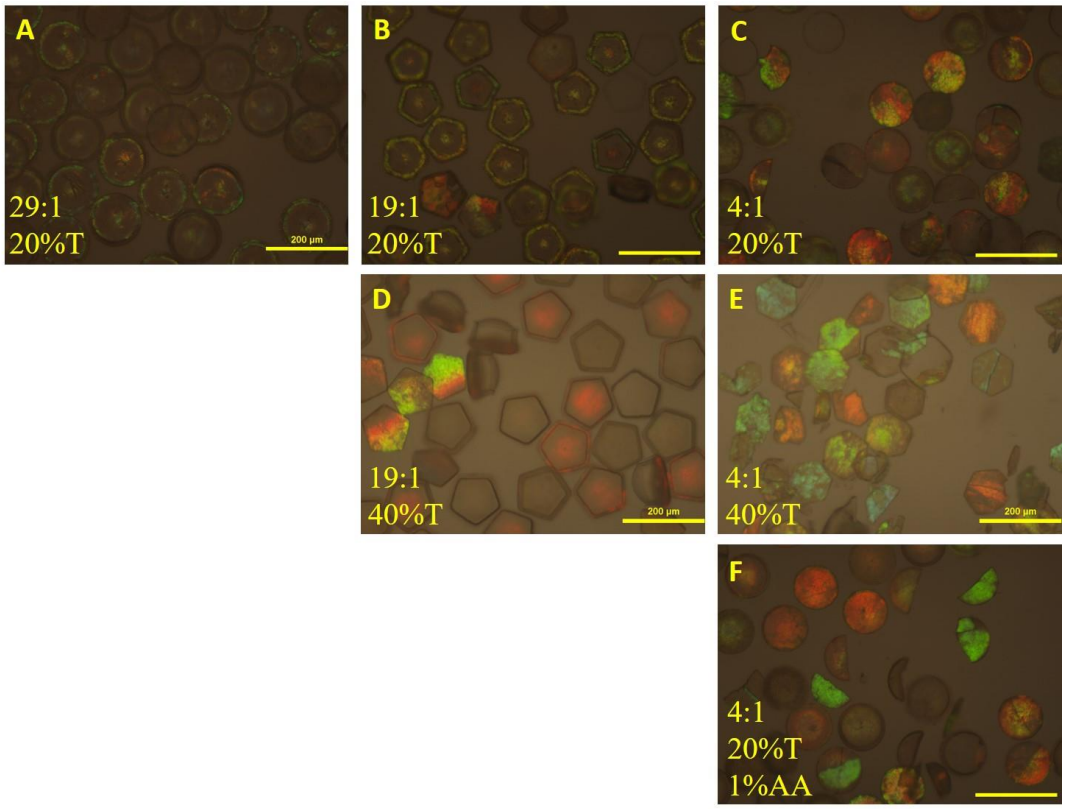

Figure 12. Opal structured hydrogel microparticles fabricated imaged via brightfield microscopy containing (A) 29:1 ratio of acrylamide to bisacrylamide and 20% total monomer content, T, (B) 19:1 with 20%T, (C) 4:1 with 20%T, (D) 19:1 with 40%T, (E) 4:1 with 40%T and (F) 4:1 with 20%T and 1% acrylic acid, AA, in the prepolymer solution.

Next I studied the effect of monomer composition on the fabrication of opal structured microparticles such as the ratio of acrylamide to bisacrylamide, the total monomer content (%T), and the addition of acrylic acid in the prepolymer solution.

To do this I prepared multiple prepolymer solutions containing different ratios of acrylamide to the cross linker bisacrylamide with varying total monomer content, 1% photoinitiator, and DI water. I put the prepolymer solution on top of the micromold containing the

deposited opal layer. The mold was then placed into a vacuum chamber to allow the prepolymer solution to seep into the wells. The excess prepolymer solution was removed from the micromold in a humidity-controlled chamber, and a cover slide was placed over the micromold to prevent evaporation of the prepolymer solution. The micromolds were then placed under a hand-held UV lamp to initiate radical chain polymerization. Next the microparticles were collected from the mold using a pipette and washed three times using DI water containing 0.05% (v/v) TW20. They were then imaged via brightfield microscopy under white light.

Figure 12A shows opal structured hydrogel microparticles fabricated with a 29:1 ratio of acrylamide to bisacrylamide with 20%T. They are non-uniform in color as there is a thin area of color around the edge of the particle with a circular area of color in the center of the particle. Figure 12B shows microparticles fabricated with a 19:1 ratio with 20%T are similar in appearance to the microparticles shown in Figure 12A. Microparticles containing 40%T with 19:1 are shown in Figure 12D. These particles are mostly red with a few showing multiple colors of yellow, green, and red.

Microparticles fabricated with a 4:1 ratio resulted in a more uniform color across each particle compared to those made with 19:1 and 29:1 ratios under the conditions examined. Figure 12C displays microparticles made with 4:1 and 20%T show color throughout the particle but are non-uniform as they contain multiple colors in one particle. The microparticles in Figure 12E, fabricated with 4:1 ratio and higher total monomer content of 40%T, are more uniform throughout each individual microparticle. There are multiple colors of microparticles such as blue, green, yellow, and orange, but each is fairly uniform within each microparticle. Finally, the results in

Figure 12F show microparticles made with 4:1 ratio, 20%T, and 1% acrylic acid (AA) are intense in color. About 40% of the microparticles show intense red or green color that is uniform throughout each individual microparticle.

The results in Figure 12 show that fabricating opal structured hydrogel microparticles using polyacrylamide as the polymer layer results in non-uniform color and a low yield of uniform colored microparticles. Based on recent studies from Professor Yi's group it was expected that acrylamide would form uniform polymer networks with minimal phase separation, thus not likely to disrupt the opal structure. However, I had difficulties obtaining uniform color in the microparticles presumably due to the slow polymerization rate of acrylamide, which takes about 30 to 60 minutes[24]. This slow polymerization rate may have contributed to non-uniformity by disrupting the PS bead layer.

In summary, fabrication of opal structured hydrogel microparticles with acrylamide and bisacrylamide as the cross-linker results in non-uniform microparticles perhaps due to the slow polymerization time.

4.6 Fabrication of opal structured hydrogel microparticles using poly(ethylene glycol) diacrylate (PEGDA) as the hydrogel layer

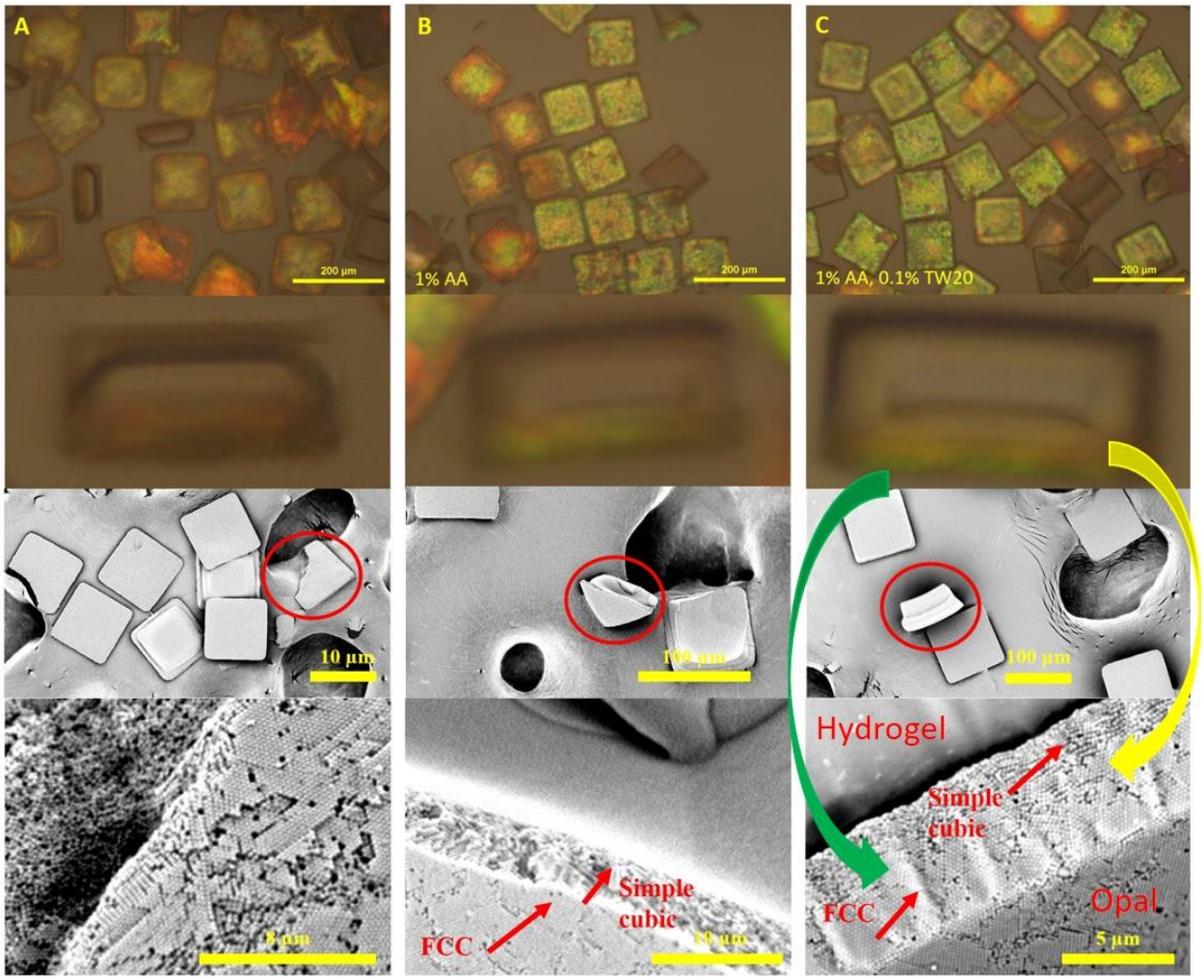

Figure 13. Opal structured hydrogel microparticles fabricated with PS10 beads and 20% poly(ethylene glycol) diacrylate (PEGDA) as the hydrogel layer with 1% photoinitiator. The microparticles were imaged via brightfield microscopy in the first and second rows and scanning electron microscopy (SEM) was used in the third and fourth rows. The microparticles were fabricated with (A) 20% PEGDA only, (B) 1% v/v acrylic acid (AA), and (C) 1% v/v AA and 0.1% v/v TW20.

I next examined the effect of fabricating the opal structured hydrogel microparticles with poly(ethylene glycol) diacrylate (PEGDA) in the prepolymer solution. The hypothesis is that the rapid polymerization of crosslinking monomer PEGDA may lead to less disruption of the assembled PS bead layers, despite our group's recent findings on phase separation[6].

To do this I prepared three prepolymer solutions. One contained only 20% PEGDA, 1% photoinitiator, and DI water. The second consisted of 20% PEGDA, 1% photoinitiator, DI water, and 1% acrylic acid (AA). The final prepolymer solution consisted of 20% PEGDA, 1% photoinitiator, DI water, 1% (v/v) AA, and 0.1% (v/v) TW20. The microparticles were fabricated by the same procedure as outlined in the previous section.

The first row of Figure 13A shows brightfield micrographs of the microparticles fabricated without AA or TW20. Most of the microparticles are uniformly yellow with no phase separation occurring and a high yield of uniform yellow microparticles (i.e. 80%). The second row in Figure 13A shows a close-up of a side view of a microparticle. Two colors can be seen in the opal layer: orange and yellow. The next image in Figure 13A was taken with a scanning electron microscopy (SEM) with a magnified image of the circled broken microparticle as the last image in the row.

The first two images in Figure 13B contain brightfield micrographs of microparticles fabricated with 1% AA in the prepolymer solution. The first row shows mostly uniform yellow-green microparticles with a few orange and yellow multicolored microparticles. The yield of yellow-green colored particles, 75%, is high, particularly when compared with acrylamide-based microparticles shown in Figure 12. The second row of Figure 13B shows a magnified image of the side view of a microparticle in the same batch, which shows the opal layer contains both a yellow-green color with a few areas of orange. The next two rows in Figure 13B are SEM images with the bottom row containing a magnified image of the broken microparticle. It shows that the bottom of the opal layer contains FCC structure followed by simple cubic structure closest to the hydrogel layer.

Finally, Figure 13C contains brightfield (first and second row) and SEM (third and fourth row) images of microparticles fabricated with 1% (v/v) AA and 0.1% (v/v) TW20 in the prepolymer solution. The first image shows a high yield, 70%, of uniform yellow-green microparticles. The second row shows a magnified view of the side of a microparticle, where two different colored opal layers are evident. The top layer, closest to the hydrogel, is yellow and the bottom layer is green. This corresponds to the next two images in Figure 13C, where the third row is a SEM image of the microparticles. The circled microparticle, which is on its side, shows the Janus nature of these opal structured hydrogel microparticles. There is a hydrogel layer on top of the opal layer. The fourth row is a zoomed-in image of the microparticle on its side, where two packing structures are noticeable: simple cubic structure near the hydrogel layer and FCC structure at the bottom of the microparticle.

The results in Figure 13 show that different PS bead assembly structures lead to different colored microparticles. This is especially evident in the last row of Figure 13C where the FCC region on the bottom of the microparticle corresponds with green and the simple cubic region is yellow.

The FCC structure resulting in green color is further evident using the modified Bragg Equation from the previous section, which is again showed here.

$$\lambda = \frac{\sqrt{8}}{\sqrt{3}} * D * \sqrt{n_{ps}^2 \phi + n_{void}^2 (1 - \phi)}$$

Equation 1. Modified Bragg Equation for FCC packing.

Where D is the diameter of PS10 beads which is 200nm from earlier calculations, n_{ps} is the refractive index of PS which is 1.5916, n_{void} is the refractive index of the void space which is primarily water in this case and is 1.3325, and ϕ is the packing factor which is 0.74 for FCC packing. Substituting the values into Equation 1 and solving for the wavelength results in a wavelength of about 500nm for FCC packing structure. Referring to the visible light spectrum shown in Figure 11 indicates 500nm results in green, which is what was shown in the second row of Figure 13C for the FCC opal layer.

The procedure can be used to calculate the wavelength of the simple cubic layer in Figure 13C using another version of the modified Bragg Equation for simple cubic structure shown below.

$$\lambda = 2 * D * \sqrt{n_{ps}^2 \phi + n_{void}^2 (1 - \phi)}$$

Equation 3. Modified Bragg Equation for simple cubic packing.

Where D is the diameter of PS10 beads which is 200nm from earlier calculations, n_{ps} is the refractive index of PS which is 1.5916, n_{void} is the refractive index of the void space which is primarily water in this case and is 1.3325, and ϕ is the packing factor which is 0.52 for simple cubic packing. Substituting the values into Equation 3 results in a wavelength of 590nm. According to Figure 11, 590nm corresponds to yellow light. Therefore, simple cubic packing structure shows yellow color as shown in Figure 13C and the modified Bragg Equation.

This clear two-layered assembly structures and their corresponding colors may be attributed to three possibilities. The first is that the bottom opal layer had more time to slowly

assemble and position into a FCC structure compared to the top layer, which most likely evaporates earlier and does not have time to position into a FCC structure. The second possibility is that the PS bead layer was disrupted by the addition of the prepolymer solution on top, which caused the top layer of PS beads to shift into a simple cubic structure. The final possibility is that the PS bead assembly structure shifted during polymerization where the polymer chains could have moved and broke the close packing. This indicates uniform opal structured hydrogel microparticles can be fabricated by minimizing the simple cubic structure or disruption of closely packed assemblies so that the opal layer is one color. Figure 13 also indicates that using PEGDA instead of polyacrylamide as the polymer system results in more uniform and colorful microparticles, presumably due to the more rapid polymerization rate of PEGDA.

In summary, the color of the microparticles is caused by the packing structure of the opal layer. FCC and simple cubic structures result in different colors in the opal layer, and to obtain uniform microparticles, the simple cubic structure should be minimized. PEGDA may be a promising polymer system to use due to its more rapid polymerization rate which results in more uniform and intense microparticles.

5. Conclusion

In this thesis, I examined various parameters for fabrication of opal structured hydrogel microparticles with uniform and intense color. First, the opal layer comprised of PS beads was deposited in a uniform manner and showed intense blue color without the use of any pigments or dyes by slowly evaporating the PS bead solution containing 40% (v/v) ethanol in a humidity-controlled chamber. Next it was demonstrated that 0.1% (v/v) TW20 was needed in the PS bead solution to reduce surface tension and improve the uniformity of the intense blue colored opal layer. Both the modified Bragg Equation and SEM images were then utilized to show that the size of the PS beads directly influences the color of the opal layer, as smaller PS beads lead to more purple color and larger PS beads result in more green color. Polyacrylamide was first used as the polymer in the hydrogel layer which was found to produce non-uniform microparticles with phase separation occurring in some cases. PEGDA in the hydrogel layer was found to be a more promising polymer as it resulted in a higher yield of more uniform and intensely colored microparticles. Finally, the color of the microparticles was found to be determined by the packing structure of the opal layer, indicating simple cubic packing structure should be minimized as much as possible. This results in uniform and intensely colored microparticles which have the potential to be used in many biosensing and medical diagnostic applications.

6. Future Directions

Although much progress has been made in fabricating uniform and intensely colored opal structured hydrogel microparticles with reliable deposition and a high yield through this thesis study, more work needs be done to improve the uniformity and examine the utility in stimuli-responsive behavior and potential for biosensing applications. Based on SEM images and the modified Bragg Equation, it was found that different packing structures result in different colored opal layer, with simple cubic packing structure being yellow and FCC being green. As mentioned in the Results and Discussion section, three possibilities for Figure 13 were identified to be the cause of the different packing structures. Therefore, the next steps would be to attempt to identify the cause of the different packing structures and try to minimize multiple packing structures from occurring in the opal layer, giving rise to more uniformly colored microparticles.

Additionally, the photonic nature of the microparticles could be demonstrated by experimenting with their color changing capabilities. It was shown in the Results and Discussion section that the microparticles can be fabricated with acrylic acid in the prepolymer solution. Acrylic acid provides carboxylate functionality to the microparticles, which impart pH-dependent swelling properties to the microparticles and hence color changes over a range of pH values in the surrounding environment. Future studies can be done to observe and quantify the color changing capabilities of these microparticles.

Finally, co-polymerization with either acrylic acid or chitosan should lead to chemical functionalities (carboxylate or primary amine) that can be harnessed to anchor probe biomolecules such as antibodies via bioconjugation reactions. Upon binding of target antigens, the change in

refractive index would lead to change in color (i.e. Modified Bragg equation, Equation 1), enabling reagentless detection of biomolecular binding events.

Combined, these future studies would make further progress in developing fabrication methods to produce a high yield of uniform opal structured microparticles with intense color for biosensing and medical diagnostic applications.

7. References

[1] Leonard, S. W., Mondia, J. P., Van Driel, H. M., Toader, O., John, S., Busch, K., ... & Lehmann, V. (2000). Tunable two-dimensional photonic crystals using liquid crystal infiltration. Physical Review B, 61(4), R2389.

[2] Dziomkina, N. V., & Vancso, G. J. (2005). Colloidal crystal assembly on topologically patterned templates. Soft Matter, 1(4), 265-279.

[3] Rhee, D. K., Jung, B., Kim, Y. H., Yeo, S. J., Choi, S. J., Rauf, A., ... & Yoo, P. J. (2014). Particle-nested inverse opal structures as hierarchically structured large-scale membranes with tunable separation properties. ACS applied materials & interfaces, 6(13), 9950-9954.

[4] Liu, E. Y., Jung, S., & Yi, H. (2016). Improved Protein Conjugation with Uniform, Macroporous Poly (acrylamide-co-acrylic acid) Hydrogel Microspheres via EDC/NHS Chemistry. Langmuir, 32(42), 11043-11054.

[5] Le Goff, G. C., Srinivas, R. L., Hill, W. A., & Doyle, P. S. (2015). Hydrogel microparticles for biosensing. European polymer journal, 72, 386-412.

[6] Jung, S., & Yi, H. (2012). Fabrication of chitosan-poly (ethylene glycol) hybrid hydrogel microparticles via replica molding and its application toward facile conjugation of biomolecules. Langmuir, 28(49), 17061-17070.

[7] Wang, Y., & Xia, Y. (2004). Bottom-up and top-down approaches to the synthesis of monodispersed spherical colloids of low melting-point metals. Nano letters, 4(10), 2047-2050.

[8] Opal. (2017). In Encyclopædia Britannica. Retrieved from http://academic.eb.com.ezproxy.library.tufts.edu/levels/collegiate/article/opal/57166

[9] Darragh, P. J., & Klein, C. (1970, January 01). Opal. Retrieved April 07, 2017, from https://doi.org/10.1036/1097-8542.469700

[10] Waterhouse, G. I., & Waterland, M. R. (2007). Opal and inverse opal photonic crystals: fabrication and characterization. Polyhedron, 26(2), 356-368.

[11] Miguez, H., Blanco, A., Lopez, C., Meseguer, F., Yates, H. M., Pemble, M. E., ... & Sanchez-Dehesa, J. (1999). Face centered cubic photonic bandgap materials based on opal-semiconductor composites. Journal of lightwave technology, 17(11), 1975-1981.

[12] Khokhar, A. Z., De La Rue, R. M., Treble, B. M., McComb, D. W., & Johnson, N. P. (2008). Stibnite inverse opal. Micro & Nano Letters, 3(1), 1-6.

[13] Norris, D. J., Arlinghaus, E. G., Meng, L., Heiny, R., & Scriven, L. E. (2004). Opaline Photonic Crystals: How Does Self-Assembly Work?. Advanced Materials, 16(16), 1393-1399.

[14] Jian, Y., He, Y., Jiang, T., Li, C., Yang, W., & Nie, J. (2013). Volume shrinkage of UV-curable coating formulation investigated by real-time laser reflection method. Journal of Coatings Technology and Research, 10(2), 231-237.

[15] Choi, D. G., Jang, S. G., Yu, H. K., & Yang, S. M. (2004). Two-dimensional polymer nanopattern by using particle-assisted soft lithography. Chemistry of materials, 16(18), 3410-3413.

[16] Wade, L. G. (2013). Organic chemistry. Upper Saddle River, N.J: Prentice Hall.

[17] Appel, E. A., del Barrio, J., Loh, X. J., & Scherman, O. A. (2012). Supramolecular polymeric hydrogels. Chemical Society Reviews, 41(18), 6195-6214.

[18] Pal, K., Banthia, A. K., & Majumdar, D. K. (2009). Polymeric hydrogels: characterization and biomedical applications. Designed monomers and polymers, 12(3), 197-220.

[19] Le Goff, G. C., Srinivas, R. L., Hill, W. A., & Doyle, P. S. (2015). Hydrogel microparticles for biosensing. European polymer journal, 72, 386-412.

[20] Butun, S., & Sahiner, N. (2011). A versatile hydrogel template for metal nano particle preparation and their use in catalysis. Polymer, 52(21), 4834-4840.

[21] γ-Ray Induced Polymerization. (n.d.). Retrieved April 07, 2017, from http://large.stanford.edu/courses/2012/ph241/weil1/

[22] Xia, Y., & Whitesides, G. M. (1998). Soft lithography. Annual review of materials science, 28(1), 153-184.

[23] Electromagnetic spectrum. (n.d.). Retrieved April 06, 2017, from https://www.pinterest.com/rosegonnella/electromagnetic-spectrum/

[24] Jung, S., Abel, J. H., Starger, J. L., & Yi, H. (2016). Porosity-Tuned Chitosan–Polyacrylamide Hydrogel Microspheres for Improved Protein Conjugation. Biomacromolecules, 17(7), 2427-2436.

[25] Neser, S., Bechinger, C., Leiderer, P., & Palberg, T. (1997). Finite-size effects on the closest packing of hard spheres. Physical review letters, 79(12), 2348.

[26] Magnetoresponsive Discoidal Photonic Crystals Toward Active Color Pigments Adv. Mater. 26, 5801-5807 (2014)